2014 IEEE International Conference on Robotics & Automation (ICRA)
Hong Kong Convention and Exhibition Center
May 31 - June 7, 2014. Hong Kong, China

Outlier Rejection for Visual Odometry using Parity Space Methods

Arun Das* and Steven L. Waslander†
University of Waterloo, Waterloo, ON, Canada, N2L 3G1

***Abstract*— Typically, random sample consensus (RANSAC) approaches are used to perform outlier rejection for visual odometry, however the use of RANSAC can be computationally expensive. The parity space approach (PSA) provides methodology to perform computationally efficient consistency checks for observations, without having to explicitly compute the system state. This work presents two outlier based rejection techniques, Group Parity Outlier Rejection and Parity Initialized RANSAC, which use the parity space approach to perform rapid outlier rejection. Experiments demonstrate the proposed approaches are able to compute solutions with increased accuracy and improved run-time when compared to RANSAC.**

I. Introduction

In situations where observed data is fitted to a parameterized model, the presence of outliers in the measurements can corrupt the solution. Many approaches exist which aim to attenuate the effect of outliers, or remove them from the measurement set all-together. The use of robust statistical methods, such as the L-estimator, M-estimator, R-estimator [1] and least median squares [2], were proposed in order to reduce the affect of outliers on the final solution. Batch heterogeneous outlier removal algorithms have also been suggested for SLAM applications [3], however the approach is mainly limited to scenarios where the number of observed measurements is small.

In order to perform outlier rejection where many measurements are observed, the RANSAC algorithm [4] is typically used, and has been successful in many computer vision [5], visual odometry (VO) [6], [7] and SLAM [8], [9] applications. Many extensions of the RANSAC algorithm have been proposed, such as Maximum Liklihood Sample Consensus (MLESAC) [10], which assumes known probability distributions of the inlier and outlier to evaluate the sample hypothesis, and Local Optimization RANSAC (LO-RANSAC) [11], where the maximum inlier set is refined at each iteration using a local optimization technique.

The general issue with the RANSAC approach is having to perform a sufficiently large number of iterations in order to achieve a model with a high confidence level. The number of required iterations can become large when the outlier ratio is high. The Random-RANSAC (R-RANSAC) approach [12], [13] was suggested to reduce the number of iterations required. In the R-RANSAC approach, the model computed from the random sample set is first verified using a small subset of the measurements prior to evaluating the fitness cost using the full observation set. Although effective, R-RANSAC still requires the computation of the model parameters at every iteration, which is computationally expensive for VO and SLAM applications.

An alternative method for outlier detection is the parity space approach (PSA), which was first developed in order to perform fault detection and isolation for instrument clusters [14], but has also been applied to fault detection for nuclear power stations [15], and in flight avionics [16]. The PSA has also been applied in a visual SLAM formulation [17], where batches of image features are tested for outliers using a PSA consistency test. Using the measurement model of the system, the PSA projects the measurements into the parity space, where the presence of outliers can be detected. Since the projection onto parity space is computed using only the measurement model, the state of the system is not required.

Visual odometry estimates the egomotion of the camera though examination of the changes that motion induces on the camera images. A typical VO approach is to use corresponding image features between successive camera frames and estimate the incremental motion, which can be successfully performed using both monocular [18], [19] and stereo cameras [7], [5], [20]. In order to provide an accurate motion estimate, feature correspondences should not contain outliers, and typically a rejection scheme such as RANSAC is used.

In this work, we propose two methods which use parity space consistency testing to perform outlier rejection and demonstrate their effectiveness when used in a VO application. In the first method, Group Parity Outlier Rejection (GPOR), a parity space test is performed on subgroups of the measurement vector, and groups which fail the test are discarded. The second method, Parity Initialized RANSAC (PI-RANSAC), improves the RANSAC algorithm by performing a parity space consistency test on the randomly selected sample set. The parity space test is computationally efficient and is shown to generate accurate parameter estimates with significantly fewer iterations when compared to RANSAC.

The GPOR and PI-RANSAC methods are validated using using the KITTI vision dataset [21]. The experiments demonstrate that the GPOR approach consistently outperforms RANSAC in terms of run-time while providing comparable accuracy in the solution, and the PI-RANSAC method is able to provide solutions with an average 44.45% increase in accuracy and an average 68.95% improvement in run-time when compared to RANSAC.

* PhD Student, Mechanical and Mechatronics Engineering, University of Waterloo; adas@uwaterloo.ca
† Assistant Professor, Mechanical and Mechatronics Engineering, University of Waterloo; stevenw@uwaterloo.ca

978-1-4799-3684-7/14/$31.00 ©2014 IEEE

II. Problem Formulation

A. Visual Odometry Method

The visual odometry algorithm used in this work was initially developed by [6] and [7]. An open source implementation is available at `http://www.cvlibs.net/software/libviso/`. A brief overview of the approach is presented here.

To determine the egomotion of the stereo camera between two successive frames, feature detection and matching is performed between the images of the stereo pair at the previous time-step to the images of the stereo-pair at the current time-step. Denote the i^{th} 3D feature point from the previous time step as $d_i \in \mathbb{R}^3$, where d_i consists of the x, y and z components of the point in the camera frame.

Given N_Y features from the previous time-step, denote the full set of 3D feature points as $Y = \{d_1, \ldots, d_{N_Y}\}$. Let the full state which defines the egomotion of the camera be denoted as $x \in \mathbb{SE}(3)$. Provided an estimate of the egomotion is available, each feature from the previous time-step can be transformed according to the egomotion estimate and re-projected back into the pixel co-ordinates of the stereo images for the current time-step. Denote the left camera reprojection mapping, $\Theta_x(d)^l : \mathbb{R}^3 \mapsto \mathbb{R}^2$ as

$$\Theta_x(d)^l = \mathcal{K}(T_x(d)), \tag{1}$$

where $\mathcal{K}$ is the camera matrix and $T_x(d) : \mathbb{R}^3 \mapsto \mathbb{R}^3$ is the transformation which maps a point, d, from the left camera frame of the previous time-step to the left camera frame in the current time step according to the egomotion state x. A re-projection mapping into the right camera image is similary denoted as $\Theta_x(d)^r$.

Denote a measurement of the feature corresponding to a point, $d_i \in Y$, in the current left image as $z^l_{d_i} \in \mathbb{R}^2$ and similarly a measurement in the current right image as $z^r_{d_i} \in \mathbb{R}^2$. Since each corresponding feature results in two measurements from the left and right image, and each measurement contains two elements for the u and v pixel co-ordinates respectively, a single feature actually provides 4 independent measurements. Using the measured features of the current frame and the re-projected feature point locations from the previous frame, a cost function, $\Lambda_Y(x) : \mathbb{SE}(3) \mapsto \mathbb{R}$, which penalizes the reprojection error over the entire set of corresponding features from feature set Y can be defined as

$$\Lambda_Y(x) = \sum_{d_i \in Y} \|z^l_{d_i} - \Theta_x(d_i)^l\|^2 + \|z^r_{d_i} - \Theta_x(d_i)^r\|^2. \tag{2}$$

Finally, the egomotion of the camera is estimated by optimizing the cost given by Equation (2) over the features contained in Y.

B. Outlier Rejection

Loosely speaking, an outlier can be defined as a measurement which, by some measure, is inconsistent with the majority of the measurements. In a typical RANSAC approach, a hypothesis model is constructed from a sample set of measurements randomly selected from the full measurement set. Each measurement is then compared to the hypothesis model and is added to an inlier consensus set if an application specific fitness measure is satisfied. In the case of visual odometry, the reprojection error for the feature must be less than a given threshold to be condsidered an inlier. The entire process of constructing hypothesis models from random samples and determining the inliers is repeated for a fixed number of iterations, while keeping track of the largest consensus set. A final model for the system can then be generated using the largest inlier consensus set.

III. Parity Space Fault Detection

In this section, a brief overview of the parity space fault detection methodology is presented. For a thorough discussion on parity space fault detection and isolation, the reader is directed to [22], [23]. Although the approach is demonstrated using a linear measurement model, it should be noted that a nonlinear measurement model, $h(x)$, can be linearized about an operating point, x_0, to generate an approximate linear model,

$$\hat{y} = \bar{H}x, \tag{3}$$

where $\bar{H}$ is the linearized measurement model, $\bar{H} = \frac{\partial h}{\partial x}|_{x_0}$, and $\hat{y} = y - h(x_0)$ are the shifted measurements according to the operating point. Although the linearization introduces a state dependent measurement matrix to the parity space approach, the linearization error is negligible assuming the chosen operating point is sufficiently close to the true state [22]. In the case of egomotion estimation using visual odometry, performing the linearization assuming zero movement between successive frames is acceptable, provided the frame-rate of the camera is sufficiently high.

A. Parity Vector Generation

Suppose that k measurements are observed at any given time-step. For a system with n states, the measurement equation is defined as

$$y = Hx + e + f, \tag{4}$$

where $y \in \mathbb{R}^k$ is the measurement vector, $H \in \mathbb{R}^{k \times n}$ is the measurement model, $x \in \mathbb{R}^n$ is the state vector, $e \in \mathbb{R}^k$ is the additive measurement noise vector, and $f \in \mathbb{R}^k$ is the fault vector which models the error in the measurements under the assumption that the measurement set contains an outlier. If y contains no outliers, the fault vector f is the zero vector. The additive measurement noise, e, is assumed to be drawn from a Gaussian distribution with zero mean and covariance $Q = \sigma_e I_{k \times k}$, where $\sigma_e \in \mathbb{R}$ is the measurement noise variance.

The parity space approach seeks to transform the measurements into a vector space, known as the *parity space* where outlier rejection can be performed. The projection of the measurements into the parity space is a linear transformation defined by the matrix $V \in \mathbb{R}^{(k-n) \times k}$, and the column space of V is defined as the parity space. For the parity space

approach, it is required that V is an orthogonal matrix that is also orthogonal to H, or

$$VH = 0, \tag{5}$$

$$VV^T = I_{(k-n)}. \tag{6}$$

Although any V which satisfies Equations (5) and (6) is sufficient, a simple method for computing V exists. Suppose the matrix $W \in \mathbb{R}^{(k-n)\times k}$ is given as

$$W = I - H(H^T H)^{-1} H^T. \tag{7}$$

If W is post multiplied by H, it is clear that Equation 5 is satisfied. To satisfy Equation 6, a Gram-Schmidt orthogonalization procedure is performed on W, resulting in an orthogonal matrix V. The *parity vector*, $p \in \mathbb{R}^{(k-n)}$, is defined as the projection of the measurements, y, onto the parity space, and can be used to determine if the measurement vector contains an outlier. Once V is known, the parity vector is calculated as $p = Vy$, and when substitued into Equation (4), the expression for the parity vector becomes $p = VHx + Ve + Vf$. Due to Equation 5, the term VHx is zero, and the state is removed from the problem. The resulting parity vector is

$$p = Ve + Vf. \tag{8}$$

With the noise assumption of $E[e] = 0$ and $E[ee^T] = Q$, if there are no outliers in the data, then the parity vector is normally distributed as $p \sim \mathcal{N}(0, VQV^T)$. In order to model an inconsistency in the measurements, assume that the i^{th} measurement is an outlier. The outlier can be modelled using the vector f by setting the i^{th} component of f, f_i to a non-zero value. Then, the parity vector is distributed as $p \sim \mathcal{N}(v_i f_i, VQV^T)$, where v_i is the i^{th} column of V. Therefore, when an outlier is present the mean of the parity vector is shifted by magnitude f_i, in the fault direction given by v_i.

B. Outlier Detection Test

Under the assumption of no outliers in the measurement vector, the magnitude of the parity vector is generally small as defined by the measurement noise Q. Conversely, when an outlier is present, the magnitude of the parity vector is dominated by the size of the fault component, f_i. Thus, the magnitude of the parity vector can be used to construct an outlier detection test statistic, and is given as $\lambda = p^T p$.

The test statistic, λ, is chi-squared (χ^2) distributed with $k-n$ degrees of freedom, therefore, a χ^2 test can be used to determine the presence of an outlier. Suppose a false alarm probability of α is desired. The critical threshold, δ, which satisfies the probability $P(\lambda > \delta) = \alpha$, can be determined using a χ^2 distribution look up table. Next, define the null hypothesis, $\mathcal{H}_0$, and the alternative hypothesis, $\mathcal{H}_1$ as

$$\mathcal{H}_0 : \ y \text{ contains no outliers}$$
$$\mathcal{H}_1 : \ y \text{ contains an outlier}$$

If $\lambda \leq \delta$, the measurements are consistent, there are no outliers present and the null hypothesis is accepted. Else, if $\lambda > \delta$, the test indicates that a there is an inconsistency in the measurements due to an outlier and the null hypothesis is rejected.

C. Probability of Missed Detection

Define the probability of missed detection, P_m as the probability that the outlier detection test declares no outliers are present when, in fact, the measurement vector contains an outlier. Generally, P_m is difficult to determine accurately as it requires the integration of the parity vector distribution which has been shifted by the fault vector $f_i v_i$, over the hypersphere defined by the detection test threshold, δ. However, an upper bound on P_m can be determined by marginalizing the parity vector distribution in the direction of the fault vector, resulting in a one dimensional distribution which can be easily integrated. The upper bound on P_m is given as

$$P_m < \int_{-\delta}^{\delta} \frac{1}{\sqrt{2\pi}} e^{-\frac{1}{2}\left(\frac{\rho - f_i}{\sigma_e^2}\right)} d\rho. \tag{9}$$

Although this is an acceptable upper bound, in cases where the parity space is relatively low ($(k-n) = 2$), it is possible to compute a tighter approximation for the upper bound by further integrating Equation 9 over the disk defined by the detection threshold, δ.

IV. Proposed Approaches

In addition to the detection of an outlier within the measurement vector, the *isolation* of the inconsistent measurement is also possible within the parity space framework [22], [23]. However, the approach is only well suited for the isolation of one outlier, where as in most visual odometry applications, the removal of multiple outliers is necessary. As such, performing the parity space outlier isolation analysis is unsuitable, and a different approach is required to handle outliers from camera feature matches.

A. Parity Group Outlier Rejection

To remove multiple outliers from the measurement vector, the Parity Group Outlier Rejection (GPOR) strategy is proposed. A similar approach is discussed in [17], however the method of selection for the group is unclear. The GPOR strategy simply divides the measurement vector into groups of size g, and performs the parity space outlier detection test on each individual group. If the test fails, all features within the group are discarded. The selection of the group size is an important parameter, as a large group size will lead to a high rate of false positives and will discard many good measurements, while a group size that is too small will increase the likelihood of including a group that contains multiple outliers that happen to be in agreement. Excessive discarding of good measurements will also occur if the outlier ratio is large, and so GPOR can be thought of as conservative in its assessment of outliers. The method is therefore most applicable for data with reasonably low outlier ratios and allows for rapid outlier removal that scales linearly with the number of measurements.

B. Parity Initialized RANSAC

Since the GPOR algorithm is best suited to measurements with a lower outlier ratio, another approach, such as RANSAC, is required for situations where a large percentage of the observations are corrupt. It is evident that the performance of the RANSAC algorithm is heavily dependent on the inlier to outlier ratio of the measurement data. When the outlier percentage is high, many RANSAC iterations are required in order to generate a correct model with sufficiently high certainty.

In certain applications, running the RANSAC algorithm for many iterations becomes computationally expensive. In the case of the presented visual odometry algorithm, a nonlinear optimization must be performed at every iteration in order to generate the candidate model from the random sample set. Furthermore, determination of the inliers using the pixel reprojection error is on the order of $O(k)$. As the number of measurements, k, can become quite large in practice, performing fewer RANSAC iterations is desirable to improve computational performance.

In order to reduce the number of required RANSAC iterations without sacrifice of solution quality, we propose the Parity Initialised RANSAC (PI-RANSAC) algorithm, where a parity space consistency check on the randomly selected measurement set is performed at each iteration. Denote the candidate sample set as S, where S is selected randomly from a uniform distribution over the entire 3D feature set, Y, such that $S \sim \mathcal{U}(Y)$ and $|S| = N_S$. Recall that each 3D point in S, d_i, is taken from the previous image-pair, and has an associated feature correspondence, z_{d_i}, in the current image-pair. To that end, define y_S as the measurement vector containing only the feature correspondences according to the points from S, or

$$y_S = [z_{d_1}^{lu}\ z_{d_1}^{lv}\ z_{d_1}^{ru}\ z_{d_1}^{rv}\ \dots\ z_{d_{N_S}}^{lu}\ z_{d_{N_S}}^{lv}\ z_{d_{N_S}}^{ru}\ z_{d_{N_S}}^{rv}]^T. \quad (10)$$

Instead of using y_S to calculate the model, as one would with a typical RANSAC approach, the PI-RANSAC algorithm performs a parity space consistency check to determine if y_S contains an outlier. If the consistency check fails, another random sample set is selected. Once the consistency test is passed, the model is computed using y_S, and the inlier set for the current iteration is determined. A feature is considered an inlier if the pixel reprojection error is less than a predefined threshold, ϵ. By using the parity based check on the random measurement sample, the computational burden of model computation and determination of the full inlier set at each iteration is replaced with a simple parity space test that is on the order of $O(c^3)$. It is important to note that although the parity check scales cubically, mainly due to computation of the V matrix, in typical applications $c << k$. The entire process is repeated for a fixed number of iterations, where upon termination, the algorithm returns the largest inlier set.

The effectiveness of the PI-RANSAC approach is dependent on the accuracy of the parity space test of the random sample set. If the parity check was 100% effective, meaning $P_m = 0$, only one PI-RANSAC iteration would be required. However, such an approach is only possible if the distribution of the fault vector is completely known, which is an unreasonable assumption in practice. In the case of outlier rejection for visual odometry, the magnitude of the fault, f_i, is unknown. However, the larger the difference between the detection threshold and the expected value of the fault magnitude, the lower the probability of a missed detection.

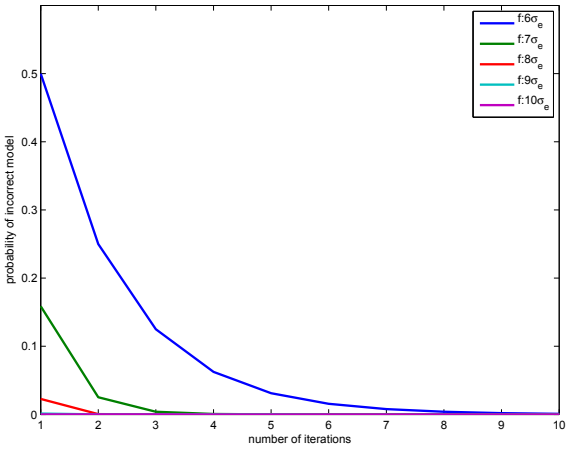

Fig. 1. Probability of the PI-RANSAC algorithm returning an incorrect model as a function of the number of performed iterations with a detection threshold of $\delta = 6\sigma_e$. Plots are shown for normalized fault vector magnitudes ranging from $f_i = \delta$ to $f_i = 10\sigma_e$.

Using the probability of a missed detection, it is possible to determine the probability the PI-RANSAC algorithm will return a bad model as a function of the number of iterations. After performing j iterations, the probability of an incorrect model, P_b, is

$$P_b = (P_m^{f_i})^j, \quad (11)$$

where $P_m^{f_i}$ denotes the probability of a missed detection from the parity space test, given a fault vector magnitude of f_i. Figure 1 illustrates the probability of returning an incorrect model as a function of the PI-RANSAC iterations performed, for a range of fault vector magnitudes. It can be seen that even when the expected value of the fault vector magnitude is equal to the parity space test detection threshold ($f_i = \delta$), the probability of returning an incorrect model is 0.0009 after only 10 iterations.

V. Experimental Results

In order to validate the proposed methods, a series of experiments are performed using camera data from the KITTI Vision Benchmark Dataset [21]. The image data is collected using two Point Grey Flea 2 cameras mounted on an automotive platform driving in urban environments. Ground truth of the vehicle motion is recorded by an OXTS RT 3003 integrated GPS/IMU, capable of providing position data at an accuracy of approximately 10 cm. The outlier rejection methods are applied to the LIBVISO2 implementation of the visual odometry method outlined in [7]. The mapping between the naming convention of the data sequences to the names as provided from the KITTI Dataset are shown in Table I.

Sequence Name	KITTI Dataset
S01	2011_09_26_drive_0067
S02	2011_09_30_drive_0016
S03	2011_09_30_drive_0020
S04	2011_09_30_drive_0027
S05	2011_09_30_drive_0033

TABLE I
SEQUENCE NAME MAPPING

Using the VO data, the Group Party Outlier Rejection (GPOR) technique, as well as the PI-RANSAC algorithm performed for 10 iterations (PR-10), is compared to the RANSAC algorithm performed with 10, 50, 100 and 1000 iterations (denoted in the tables as R-10,R-50,R-100,R-1000). The incremental motion computed between frames using each outlier rejection techniques is integrated over the test sequence to recover the egomotion of the camera, and is compared to the provided ground truth. To determine the effect which the number of features has on the outlier rejection techniques, the experiments are performed using small and large feature sets. The number of features is controlled by increasing the maximum number of allowable features maintained by the bucketing algorithm [6]. Other than the number of features and RANSAC iterations, all other parameters for the visual odometry are set to the default values. For the PI-RANSAC implementation, the detection threshold is set to $\delta = 0.5$ and for the GPOR method the group size was set to $g = 3$. The results from the experiments for the small and large feature sets are presented in Tables II and III, respectively.

For the small feature number experiment, the PI-RANSAC approach computes the solution with the least average position error, for all five test sequences. Although the average position error should generally decrease as the number of RANSAC iterations is increased, in some cases a large number of RANSAC iterations returns an *accidental* largest consensus set which does not accurately reflect the state of the system [24]. To that end, the PI-RANSAC approach is compared to the best solution discovered by RANSAC over 10, 50, 100 and 1000 iterations. In Tables II and III, the percent improvement of the PI-RANSAC solution over the best RANSAC solution is computed using the bold quantities. It is evident that the PI-RANSAC approach is very effective, as after only 10 iterations it was able to compute a solution with an average 44.45% increase in accuracy and an average 68.95% improvement in run-time compared to the best RANSAC solutions.

A similar trend is seen with the experiments performed on the large feature data set, with the exception of R-1000 for the S02, sequence, where the average position error for R-1000 is marginally better compared to PR-10. Significant computational benefit is seen for the PI-RANSAC method on the large feature sets, as in the best case a 97.19% speed-up was observed when compared to RANSAC. Although the GPOR method did not produce the solutions with the best accuracy relative to ground truth, the average position errors are indeed comparable to both PI-RANSAC and RANSAC, and consistently achieved the best run-time in all test cases.

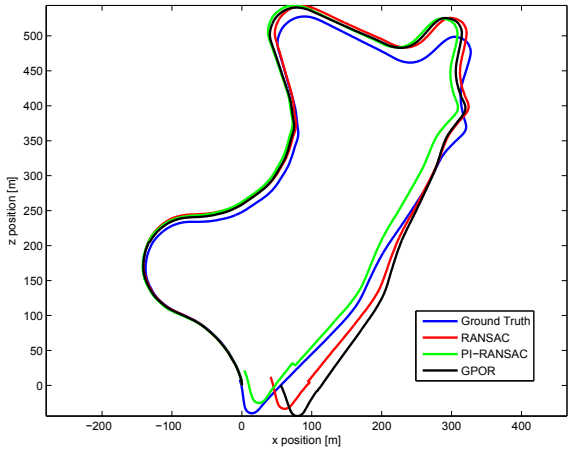

Fig. 2. Vehicle motion generated using visual odometry and outlier rejection techniques for S05.

Example plots comparing the calculated vehicle motion trajectory using GPOR, R-10, and PR-10 for sequence S05 is presented in Figure 2.

One issue with evaluation of the integrated visual odometry motion is that a poor solution in the middle of the sequence of position estimates will affect all subsequent positions. Thus, the relative error between the frame to frame positions and relative motion derived from the ground truth are computed, and summary statistics are presented in Table IV, for both small and large feature counts. As the grouping for the GPOR method is based purely on the measurement vector, the test may have a tendency to reject a high percentage of good measurements when the outlier ratio is large. It is apparent that for the sequences with large feature counts, GPOR produced the solutions with the smallest average relative error. The result suggests that it is possible to use a large number of measurments with a low outlier ratio to attenuate the effect of feature deprivation. In such cases, a simple test such as GPOR can rapidly produce accurate solutions and can outperform RANSAC methods in both accuracy and runtime.

VI. CONCLUSION

This work presents two outlier rejection approaches, GPOR and PI-RANSAC that are based within the parity space framework, and applies them to a stereo camera based VO application. The GPOR algorithm allows for rapid outlier rejection by performing parity space tests to subgroups of features of the measurement vector, resulting in a fast outlier removal strategy that scales linearly with the number of measurements. The PI-RANSAC algorithm improves upon RANSAC by performing a fast parity space consistency test on the random sample of measurements and ensures only consistent samples are evaluated for the maximum inlier set. Future work includes thorough analysis of parity space approach with nonlinear models, evaluation using synthetic data with known outlier ratios, and application of the proposed methods on problems such as SLAM and point cloud registration.

	S01	S02	S03	S04	S05
avg. feature count	299	211	234	292	245
Average Position Error (m)					
GPOR	8.59	2.64	8.82	13.75	22.00
PR-10	**7.39**	**0.89**	**4.39**	**3.43**	**19.81**
R-10	20.19	3.39	8.78	9.75	28.75
R-50	14.36	2.03	9.53	**9.05**	27.63
R-100	**12.14**	3.17	7.95	10.04	**26.04**
R-1000	13.46	**1.90**	**7.83**	12.89	30.49
Improvement (%)	39.13	53.16	43.93	62.10	23.92
Average Run Time (ms)					
GPOR	0.95	0.70	0.74	0.85	0.79
PR-10	**2.80**	**4.00**	**4.80**	**4.00**	**4.60**
R-10	1.30	1.00	1.00	1.30	1.00
R-50	6.40	4.80	5.10	**5.60**	5.00
R-100	**12.10**	90.0	9.50	11.00	**13.00**
R-1000	68.70	**30.0**	**40.0**	70.60	56.00
Speed-Up (%)	76.86	86.67	88.00	28.57	64.62

TABLE II

ACCURACY AND RUNTIME COMPARISON USING A SMALL FEATURE SET (LESS THAN 300 FEATURES ON AVERAGE).

	S01	S02	S03	S04	S05
avg. feature count	2070	1320	1231	1594	1408
Average Position Error (m)					
GPOR	3.18	3.09	6.24	12.23	22.75
PR-10	**6.61**	**1.62**	**6.82**	**6.20**	**18.67**
R-10	14.31	3.56	14.66	10.72	23.29
R-50	9.75	3.01	8.79	10.01	**21.00**
R-100	10.97	1.57	**7.75**	10.03	21.79
R-1000	**9.26**	**1.56**	10.70	**7.95**	21.60
Improvement (%)	28.62	-3.85	12.00	22.02	11.11
Average Run Time (ms)					
GPOR	6.50	4.10	3.70	5.10	4.50
PR-10	**9.90**	**8.80**	**8.30**	**12.10**	**9.30**
R-10	8.20	5.40	5.00	6.30	5.60
R-50	38.10	25.10	22.80	30.90	**26.40**
R-100	70.90	45.30	**43.40**	58.40	50.90
R-1000	**352.60**	**188.60**	161.60	**341.30**	256.30
Speed-Up (%)	97.19	95.33	80.88	96.45	64.77

TABLE III

ACCURACY AND RUNTIME COMPARISON USING A LARGE FEATURE SET (GREATER THAN 1000 FEATURES ON AVERAGE).

Average Relative Position Error (m)					
	S01	S02	S03	S04	S05
avg. feature count	299	211	234	292	245
GPOR	**0.049**	0.090	0.084	0.060	**0.082**
PR-10	0.051	0.086	**0.060**	**0.042**	0.088
R-10	0.091	0.103	0.097	0.061	0.115
R-50	0.064	0.094	0.096	0.065	0.104
R-100	0.060	0.091	0.079	0.060	0.104
R-1000	0.601	**0.085**	0.078	0.072	0.103
Average Relative Position Error (m)					
avg. feature count	2070	1320	1231	1594	1408
GPOR	**0.038**	**0.083**	**0.064**	**0.056**	**0.082**
PR-10	0.051	0.096	0.087	0.058	0.083
R-10	0.069	0.111	0.078	0.061	0.089
R-50	0.052	0.091	0.094	0.064	0.102
R-100	0.052	0.073	0.083	0.061	0.117
R-1000	0.048	0.087	0.101	0.060	0.107

TABLE IV

COMPARISON OF AVERAGE FRAME BY FRAME RELATIVE ERROR FOR BOTH SMALL AND LARGE AVERAGE FEATURE COUNTS.

REFERENCES

[1] P. Huber, *Robust Statistics*. New York: Wiley, 1974.

[2] P. J. Rousseeuw, "Least median of squares regression," *Journal of the American statistical association*, vol. 79, no. 388, pp. 871–880, 1984.

[3] C. H. Tong and T. D. Barfoot, "Batch heterogeneous outlier rejection for feature-poor slam," in *IEEE International Conference on Robotics and Automation (ICRA)*, Shanghai, China, May 2011, pp. 2630–2637.

[4] M. A. Fischler and R. C. Bolles, "Random sample consensus: a paradigm for model fitting with applications to image analysis and automated cartography," *Communications of the ACM*, vol. 24, no. 6, pp. 381–395, June 1981.

[5] R. I. Hartley and A. Zisserman, *Multiple View Geometry in Computer Vision*, 2nd ed. Cambridge University Press, 2004.

[6] B. Kitt, A. Geiger, and H. Lategahn, "Visual odometry based on stereo image sequences with RANSAC based outlier rejection scheme," in *IEEE Intelligent Vehicles Symposium (IVS)*, San Diego, CA, June 2010, pp. 486–492.

[7] A. Geiger, J. Ziegler, and C. Stiller, "Stereoscan: Dense 3D reconstruction in real-time," in *IEEE Intelligent Vehicles Symposium (IVS)*, Baden-Baden, Germany, June 2011, pp. 963–968.

[8] B. Morisset, R. B. Rusu, A. Sundaresan, K. Hauser, M. Agrawal, J.-C. Latombe, and M. Beetz, "Leaving flatland: Toward real-time 3D navigation," in *IEEE International Conference on Robotics and Automation (ICRA)*, Kobe,Japan, may 2009, pp. 3786 –3793.

[9] G. Klein and D. Murray, "Parallel tracking and mapping for small AR workspaces," in *IEEE International Symposium on Mixed and Augmented Reality (ISMAR)*, Nara, Japan, November 2007, pp. 225–234.

[10] P. H. S. Torr and A. Zisserman, "MLESAC: a new robust estimator with application to estimating image geometry," *Journal of Computer Vision and Image Understanding*, vol. 78, no. 1, pp. 138 – 156, 2000.

[11] O. Chum, J. Matas, and S. Obdrzalek, "Enhancing RANSAC by generalized model optimization," in *Asian Conference on Computer Vision (ACCV)*, Jeju, Korea, January 2004, pp. 812–817.

[12] J. Matas and O. Chum, "Randomized RANSAC with sequential probability ratio test," in *IEEE International Conference on Computer Vision (ICCV)*, Beijing, China, October 2005, pp. 1727–1732.

[13] O. Chum and J. Matas, "Randomized RANSAC with T(d,d) test," in *British Machine Vision Conference (BMVC)*, Cardiff, UK, September 2002, pp. 448–457.

[14] I. E. Potter and M. C. Sunman, "Threshold-less redundancy management with arrays of skewed instruments," AGARD, Tech. Rep. AGARDOGRAPH-224 (pp 15-25), 1977.

[15] M. D. Asok Ray and J. Deyst, "Fault detection and isolation in a nuclear reactor," *Journal of Energy*, vol. 7, no. 1, pp. 79–85, 1983.

[16] S. Hall, P. Motyka, E. Gai, and J. J. Deyst, "In-flight parity vector compensation for FDI," *Transactions on Aerospace and Electronic Systems*, vol. AES-19, no. 5, pp. 668–676, 1983.

[17] D. Tornqvist, T. Schon, and F. Gustafsson, "Detecting spurious features using parity space," in *IEEE International Conference on Control Automation, Robotics and Vision (ICARCV)*, Hanoi, Vietnam, December 2008, pp. 353–358.

[18] D. Nister, O. Naroditsky, and J. Bergen, "Visual odometry for ground vehicle applications," *Journal of Field Robotics*, vol. 23, no. 1, pp. 3–20, 2006.

[19] J.-P. Tardif, Y. Pavlidis, and K. Daniilidis, "Monocular visual odometry in urban environments using an omnidirectional camera," in *IEEE International Conference on Intelligent Robots and Systems (IROS)*, Nice, France, September 2008, pp. 2531–2538.

[20] A. Comport, E. Malis, and P. Rives, "Accurate quadrifocal tracking for robust 3D visual odometry," in *IEEE International Conference on Robotics and Automation (IROS)*, San Diego,CA, October 2007, pp. 40–45.

[21] A. Geiger, P. Lenz, C. Stiller, and R. Urtasun, "Vision meets robotics: The kitti dataset," *International Journal of Robotics Research*, vol. 32, no. 11, pp. 1231–1237, 2013.

[22] F. Gustafsson, "Statistical signal processing approaches to fault detection," *Annual Reviews in Control*, vol. 31, no. 1, pp. 41–54, 2007.

[23] F. Gustafsson and F. Gustafsson, *Adaptive filtering and change detection*. Wiley Londres, 2000, vol. 1.

[24] Q. Fan, "Matching slides to presentation videos," Ph.D. dissertation, Department of Computer Science, University of Arizona, 2008.